Measurement 62 (2015) 97–107

Contents lists available at ScienceDirect

Measurement

journal homepage: www.elsevier.com/locate/measurement

Predictions of corrosion current density and potential by using chemical composition and corrosion cell characteristics in microalloyed pipeline steels

Neda Narimani [a], Bahram Zarei [b], Hesam Pouraliakbar [b,c], Gholamreza Khalaj [d,*]

[a] School of Metallurgy and Materials Science, College of Engineering, University of Tehran, Tehran, Iran
[b] Institute of Mechanics, Faculty of Engineering, Enghelab-Eslami Center, Technical and Vocational University, Yaft Abad, Tehran, Iran
[c] Department of Advanced Materials, WorldTech Scientific Research Center (WT-SRC), Tehran, Iran
[d] Young Researchers and Elites Club, Saveh Branch, Islamic Azad University, Saveh, Iran

ARTICLE INFO

Article history:
Received 23 May 2014
Received in revised form 3 November 2014
Accepted 14 November 2014
Available online 21 November 2014

Keywords:
Artificial neural network
Electrochemical polarization
Microalloyed steel
Corrosion properties
Alkaline media

ABSTRACT

Artificial neural networks with feed forward topology and back propagation algorithm were employed to predict the effects of chemical composition and corrosion cell characteristics on both corrosion current density and potential of microalloyed pipeline steels. Doing this, the chemical compositions comprising of *"carbon"*, *"magnesium"*, *"niobium"*, *"titanium"*, *"nitrogen"*, *"molybdenum"*, *"nickel"*, *"aluminum"*, *"copper"*, *"chromium"*, *"vanadium"* and *"carbon equivalent"* (all in weight percentage) along with corrosion cell characteristics of *"reference electrode"*, *"scan rate"*, *"temperature"*, *"relative pressure of oxygen"*, *"pressure of purged CO_2"*, *"chloride ion"*, as well as, *"bicarbonate concentration"* were considered together as the input parameters of the network while the *"corrosion current density"* and *"corrosion potential"* were considered as the outputs. For purpose of constructing the models, 87 different data were gathered from literatures wherein different examinations were performed. Then data were randomly divided into training, testing and validating sets. Scatter plots and statistical criteria of *"absolute fraction of variance (R^2)"*, and *"mean relative error (MRE)"* were used to evaluate the prediction performance and universality of the developed models. Based on the analyses, the proposed models could be further used in practical applications and corrosion monitoring of the microalloyed steels.

1. Introduction

Pipelines are one of the most convenient means of transporting natural gas and crude oil from production sites to the consumer. They are efficient, economic and can last for several decades. In common, High Strength Low Alloy (HSLA) steels, also known as micro-alloyed steels, have been recognized as the mostly utilized steels for pipeline construction in the petroleum industry. These steels have been evolved in order to attain the required mechanical properties and fulfill the diameter and thickness in designs of such pipelines [1]. To obtain the former characteristics, steel makers produce these steels with a wide range of microstructures and chemical compositions developed by various manufacturing processes. The American Petroleum Institute (API) classifies pipeline steels used in hydrocarbon production and transport environments as API 5LX steels [2].

As with any other engineering structure, pipelines are subjected to service failures, due to corrosion, in oil and gas transporting media. The major focus of corrosion research in HSLA steels has been devoted for investigating

* Corresponding author. Tel.: +98 912 617 6472.
E-mail addresses: gh.khalaj@iau-saveh.ac.ir, gh_khalaj@yahoo.com (G. Khalaj).

http://dx.doi.org/10.1016/j.measurement.2014.11.011
0263-2241/

their capability to resist the localized attack of the well known forms of cracking such as Stress Corrosion Cracking (SCC), Sulfide Stress Cracking (SSC), and Hydrogen Induced Cracking (HIC) [3–5].

It is well acknowledged in the literature that different types of localized attack i.e. SCC and pitting, have several features in common. A quite number of studies revealed that SCC and pitting were associated in adjacent and/or overlapping potential ranges [6] while SCC in HSLA steels took place from initiated corrosion pits due to the stress intensification in carbonate/bicarbonate environments containing chloride ions [7]. However, limited studies have been conducted to address the corrosion behavior of these steels, especially newer generation of steels, with a particular focus on pitting.

Localized corrosion in carbonate/bicarbonate (CO_3^{2-}/HCO_3^-) environments is a great concern in the oil industry. CO_3^{2-}/HCO_3^- media results from the practice of pumping CO_2 saturated water into wells to enhance oil recovery and reduce the viscosity of the pumped fluid. The presence of CO_2 leads to the formation of a weak carbonic acid (H_2CO_3) which drives CO_3^{2-}/HCO_3^- corrosion reactions.

Potentiodynamic polarization is a direct electrochemical measurement utilized for investigating the corrosion performance. In that technique, *corrosion current density* and *potential* are extrapolated from the polarization profiles scanned across the cathodic and anodic regimes. With respect to the selected polarization ranges and potential scan rates, the characteristic performance of the tested material is revealed in a specific environmental condition as an electrochemical fingerprint. Potentiodynamic polarization is employed widely for investigating many aspects of carbon dioxide corrosion behavior of pipeline steels at different environmental conditions [8–10]. In Mohorich et al.'s work [11] which is selectively shown in Fig. 1, potentiodynamic polarization technique provided a better understanding of the effect of the bicarbonate content and temperature, as well as, silicate and chloride contents.

The final microstructure of HSLA line pipe steels is determined by its chemical composition and the thermo-mechanical treatments employed during the production processes. By considering that the design criteria are mainly focused on the properties such as mechanical resistance, toughness, as well as, weldability, the corrosion resistance, as another important factor, is also considered. The microstructure is demonstrated to have a significant effect on how firmly the corrosion scale sticks to the surface. The adherence of the corrosion product film and hence its protectiveness, has often been related to the presence of iron carbide and its morphology (laminar, globular, etc.). At the present there is no common agreement about the mechanism and the way in which microstructure and heat treatment affect the growth and stability of iron carbonate film. Stegmann et al. [12] addressed the role of temperature, chloride additives and the metallurgy on the flow induced localized corrosion. They used steel tubes with six dissimilar compositions and they found a better corrosion resistance for the quenched and tempered samples compared to the ferrite-pearlite ones. Ueda and Takabe [13] also studied the effect of the environmental factors and microstructure on the morphology of the corrosion products in bicarbonate/carbonate systems having 5 wt% NaCl. They used two different steels of J55 and N80. The J55 specimens had ferrite/pearlite microstructure while the N80 ones contained tempered martensite. The authors found that N80 steel showed a lower corrosion rates than J55 steel but suffered pitting corrosion.

In addition to the chemical composition and microstructure, environmental factors influence corrosion could be summarized as follows:

1. ***Temperature:*** It is widely recognized that the uniform CO_2 corrosion rates are accelerated by the higher temperature wherein the governing kinetics are enhanced and the associated transport processes are advanced.
2. ***Carbon dioxide partial pressure:*** CO_2 partial pressure is the key factor that controls the concentrations of the corrosive species, pH levels, the corrosive significance of many physical and chemical factors, and consequently the corrosion rates [14,15].
3. ***Dissolved oxygen:*** Oxygen induces noticeable changes in the passivation and corrosion products. While properties depend on P_{CO2}, different oxide phases could exist with variant proportions [16].

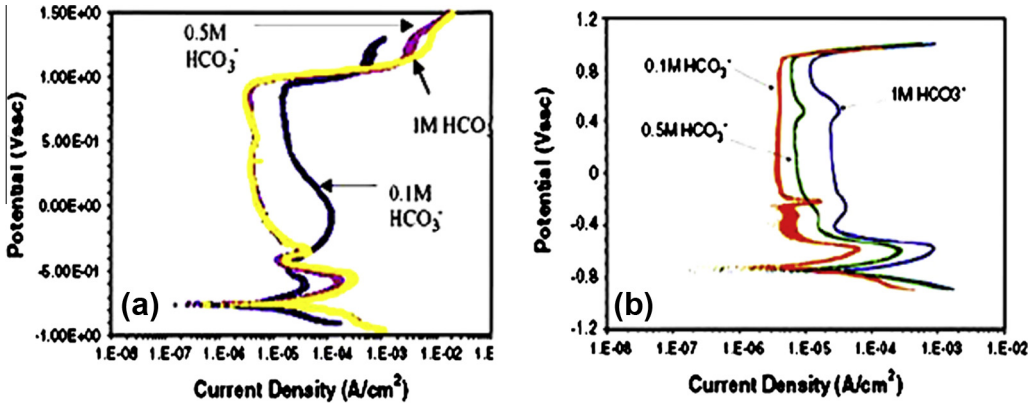

Fig. 1. Potentiodynamic scans obtained for API X70 steel in 0.1 M, 0.5 M, and 1 M bicarbonate solutions at different temperatures: (a) at 25 °C and (b) at 45 °C [11].

Table 1
Chemical composition of the six microalloyed steels investigated in this study (the values in the brackets indicate the references for the experimental data).

Steel	Chemical composition (wt%)												Ref.
	C	Mn	Nb	Ti	N	Mo	Ni	Al	Cu	Cr	V	CE_{IIW}	
X70	0.084	1.64	0.037	0.019	0.004	0.012	0.044	0.034	0.029	0.043	0.001	0.37	A
X70	0.063	1.533	0.042	0.011	0.0041	0.09	0.15	0.029	0.097	0.03	0.05	0.36	B
X100	0.1	1.66	0.043	0.02	–	0.19	0.13	0.02	0.25	0.016	0.003	0.47	[23]
X80	0.06	1.65	0.034	0.012	0.005	0.24	–	–	–	–	–	0.383	[24]
X80	0.09	1.55	–	0.0461	–	0.002	0.0001	0.0363	0.0193	0.022	0.0109	0.356	[25]
X100	0.07	2.19	–	0.01	–	0.2	0.1	0.0257	0.3	0.02	0.0096	0.507	[25]

4. ***pH level:*** pH level is an important environmental factor considered in the corrosion mechanisms and other associated physical processes control the CO_2 corrosion reactions.
5. ***Bicarbonate concentration:*** The corrosion rates were found to be proportional with the greater bicarbonate content [17] and the shapes of polarization curves showed changes accordingly [18].

Corrosion of pipeline steels in CO_2-saturated media was reported in many studies as a complex phenomenon requiring great research efforts to investigate its mechanisms and the associated determining steps. Many views were proposed, but however, they were for describing the corrosion reactions in specific cases and they were not also widely recognized [14]. This project primarily intends to provide an understanding and also a comparison on the electrochemical polarization behaviors of microalloyed steels in bicarbonate/chloride media of various concentrations.

The prediction of corrosion behavior of pipeline steels is a sophisticated task and needs a deep knowledge of whole processing parameters. Recently, artificial neural networks (ANNs) have been widely used for investigating the correlation between final properties and the chemical composition and/or processing parameters of different steel types [19–22]. As authors' literature survey, there is no work investigating the combined effects of steel chemical compositions and microstructure along with electrochemical cell setup, on corrosion current density and corrosion potential of microalloyed steels. In addition to the examined data acquired from two different API grade HSLA steels from different manufacturers, also 87 potentiodynamic polarization data were collected from literature, trained, tested and validated by neural network approach. The obtained results were compared to experimental ones to evaluate the employed approach's power for predicting the effects of mentioned parameters on the corrosion of the studied steels.

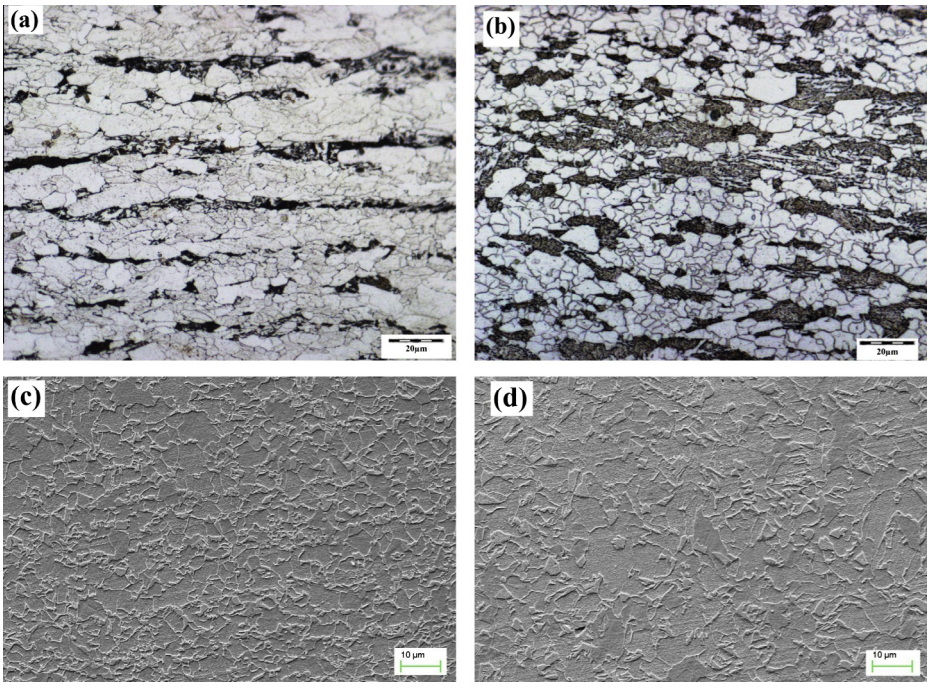

Fig. 2. Bimodal ferritic-pearlitic microstructure of API X70 microalloyed steels acquired by (a) and (b) optical and (c) and (d) scanning electron microscope while (a) and (c) belong to type A steel and (b) and (d) belong to type B steel.

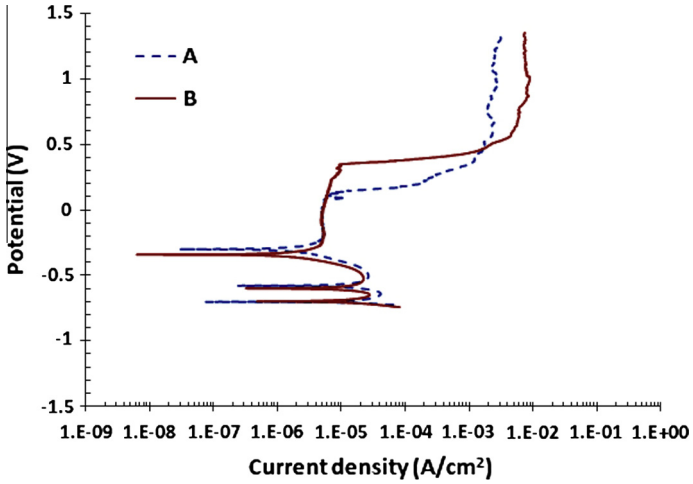

Fig. 3. The potentiodynamic scans of different API X70 steels in aerated solution containing 0.5 M carbonate and 0.01 M chloride concentrations.

2. Experimental procedures

2.1. Specimen preparation

Two API X70 grade pipeline steels supplied by the Dillinger-Hutte and Posco, named type A and type B steels, respectively, were used as test materials in this study. Rectangular flat specimens of 25 mm × 20 mm × 1 mm dimensions were machined as the working electrode from the steels for further examinations. Chemical compositions of the specimens are listed in Table 1. Prior to each experiment, the working electrode's surface was treated as the following steps:

- wet-ground up to 1200-grit emery silicon carbide (SiC) finish;
- degreased ultrasonically with acetone in the bath of distilled water for 10 min;
- rinsed with double distilled water;
- dried in a stream of cool air;
- finally, immersed in the solution.

2.2. Test solutions

Test solution was prepared from distilled water and analytical-grade reagents. The 0.5 M sodium bicarbonate ($NaHCO_3$) solution with the pH value of 9.2 was used in the tests. To investigate the effects of chloride ions (Cl^-) on pitting corrosion in bicarbonate solutions, Cl^- ions were added to $NaHCO_3$ solution in the form of sodium chloride (NaCl) to yield concentration of 0.01 M.

2.3. Electrochemical cell setup

Electrochemical testing was conducted in a standard glass cell containing the working electrode (specimen) and a platinum counter electrode. Potentials were measured with respect to an external mercury/mercurous chloride (Hg/Hg_2Cl_2) reference electrode interfaced to the test solution via a salt bridge assembly consisting of the test solution and a simulated Luggin-type polyethylene capillary which was terminated ~2 mm from the specimen.

Potentiodynamic tests were carried out using a computer-controlled electrochemical interface (potentiostat) allowing continuous monitoring of potential (E), total current (I), and time (t). Average current density (i) was obtained by dividing (I) by the initial working area of the specimen. After allowing the specimen to attain a stable open circuit potential (E_{op}), the electrode potential was swept potentiodynamically at a rate of 1.0 mV s^{-1} (unless otherwise indicated) from the initial potential of −0.6 V vs. E_{op} to the final potential of 1 V vs. Hg/Hg_2Cl_2 electrode. All potentials reported in this paper were measured with respect to Hg/Hg_2Cl_2 electrode (E = 0.221 V vs. standard hydrogen electrode (SHE)).

The potentiodynamic polarization curves were obtained for two different API X70 grade of HSLA steels at 27 ± 2 °C. It was allowed the determination of various regions of potential characteristics (anodic dissolution,

Table 2
Electrochemical parameters of the active dissolution and passive regions for type A and type B steels.

Steel type	I_{corr} (μA cm^{-2})	I_{pass} (μA cm^{-2})	Corrosion rate (mpy)	β_a (V dec^{-1})	β_c (V dec^{-1})	E_{corr} (mV(SCE))	E_{pass} (mV(SCE))	ΔE_{pass} (mV(SCE))	E_{pit} (mV(SCE))
A	1.5	5.1	0.69	70.3	−91	−0.299	−0.197	0.324	0.127
B	2	5	0.92	82.8	−60	−0.343	−0.16	0.51	0.35

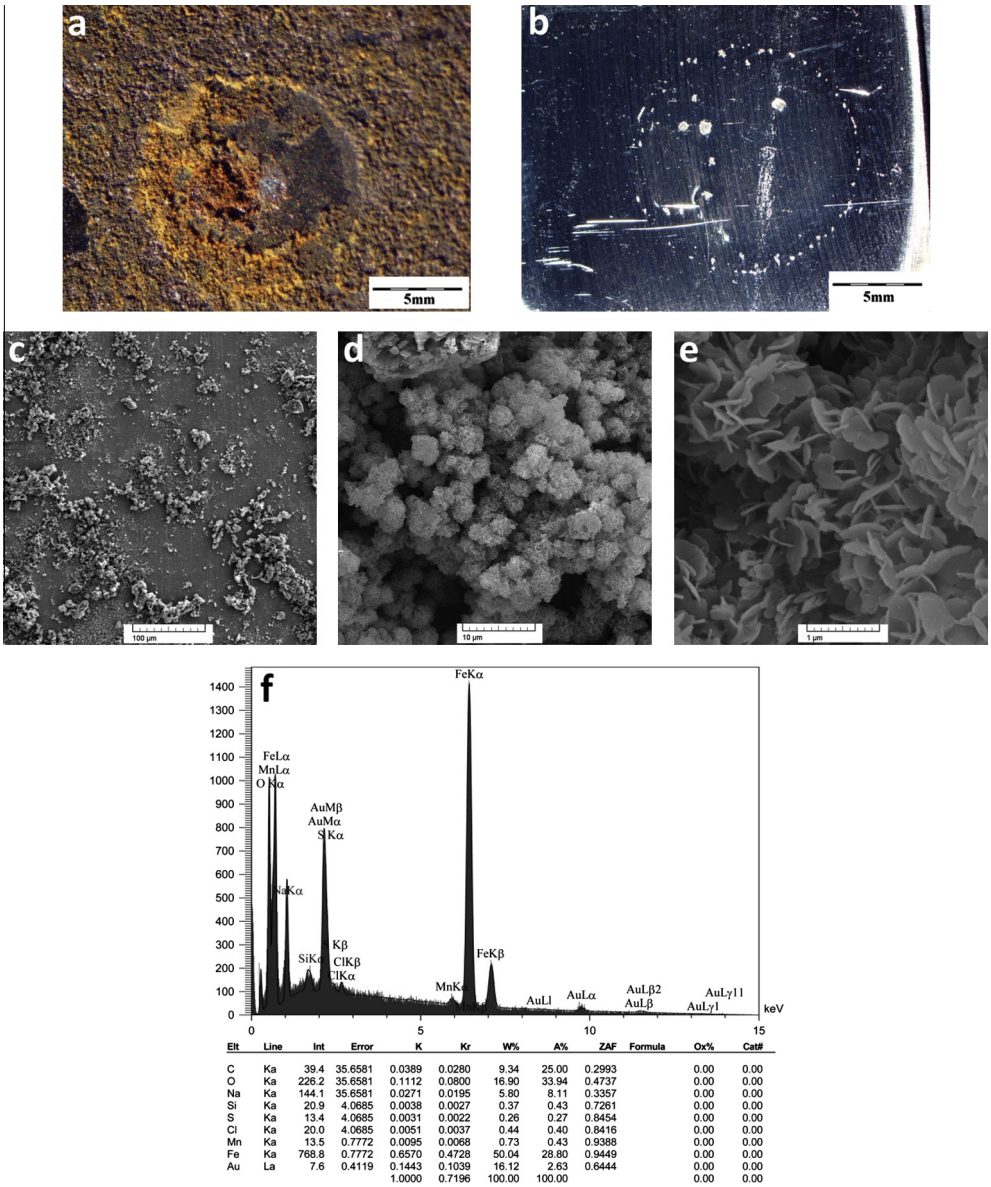

Elt	Line	Int	Error	K	Kr	W%	A%	ZAF	Formula	Ox%	Cat#
C	Ka	39.4	35.6581	0.0389	0.0280	9.34	25.00	0.2993		0.00	0.00
O	Ka	226.2	35.6581	0.1112	0.0800	16.90	33.94	0.4737		0.00	0.00
Na	Ka	144.1	35.6581	0.0271	0.0195	5.80	8.11	0.3357		0.00	0.00
Si	Ka	20.9	4.0685	0.0038	0.0027	0.37	0.43	0.7261		0.00	0.00
S	Ka	13.4	4.0685	0.0031	0.0022	0.26	0.27	0.8454		0.00	0.00
Cl	Ka	20.0	4.0685	0.0051	0.0037	0.44	0.40	0.8416		0.00	0.00
Mn	Ka	13.5	0.7772	0.0095	0.0068	0.73	0.43	0.9388		0.00	0.00
Fe	Ka	768.8	0.7772	0.6570	0.4728	50.04	28.80	0.9449		0.00	0.00
Au	La	7.6	0.4119	0.1443	0.1039	16.12	2.63	0.6444		0.00	0.00
				1.0000	0.7196	100.00	100.00			0.00	0.00

Fig. 4. Micrographs and chemical analysis of the corrosion products obtained from potentiodynamic polarization of type A steel; (a) and (b) optical microscope images, (c–e) scanning electron microscope images with different magnifications and (f) EDS chemical analysis of corrosion products.

pre-passivation, passivation, and trans-passivation) of each of tested steel. The potential for stable pitting (E_{pit}) was determined by noting the potential at which a sharp increase in the anodic current occurred, indicating sustained localized breakdown of the passive film of the tested material.

2.4. Data collection

In the present investigation, the artificial neural network has been trained, tested and validated for predicting the corrosion behavior of microalloyed pipeline steels. For this purpose, in addition of steels mentioned before, the experimental data of three microalloyed pipeline steels with different chemical compositions and microstructure have been employed [23–25]. The chemical compositions of steels are summarized in Table 1.

3. Results and discussion

3.1. Potentiodynamic polarization tests

Fig. 2(a) and (b) illustrates the microstructure of an as-received API X70 test material obtained from a sample wet-ground up to 1200-grit emery finish, successively polished with 6 and 1 µm diamond suspensions and etched with 2 vol% natal solution. The microstructures consisted of ferrite and pearlite phases. There was also an indication of the presence of a small amount of the bainitic structure.

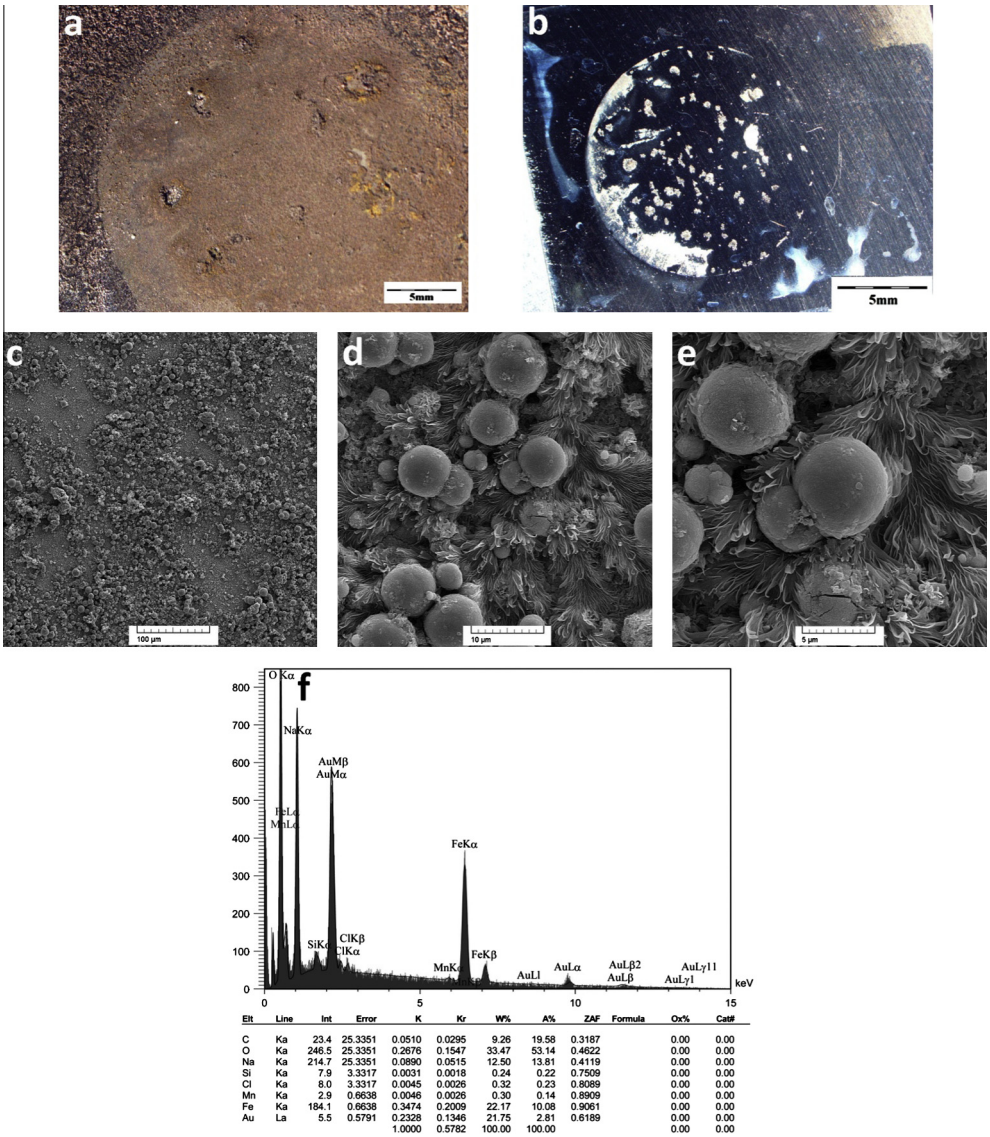

Elt	Line	Int	Error	K	Kr	W%	A%	ZAF	Formula	Ox%	Cat#
C	Ka	23.4	25.3351	0.0510	0.0295	9.26	19.58	0.3187		0.00	0.00
O	Ka	246.5	25.3351	0.2676	0.1547	33.47	53.14	0.4622		0.00	0.00
Na	Ka	214.7	25.3351	0.0890	0.0515	12.50	13.81	0.4119		0.00	0.00
Si	Ka	7.9	3.3317	0.0031	0.0018	0.24	0.22	0.7509		0.00	0.00
Cl	Ka	8.0	3.3317	0.0045	0.0026	0.32	0.23	0.8089		0.00	0.00
Mn	Ka	2.9	0.6638	0.0046	0.0026	0.30	0.14	0.8909		0.00	0.00
Fe	Ka	184.1	0.6638	0.3474	0.2009	22.17	10.08	0.9061		0.00	0.00
Au	La	5.5	0.5791	0.2328	0.1346	21.75	2.81	0.6189		0.00	0.00
				1.0000	0.5782	100.00	100.00			0.00	0.00

Fig. 5. Micrographs and chemical analysis of the corrosion products obtained from potentiodynamic polarization of type B steel; (a) and (b) optical microscope images, (c–e) scanning electron microscope images with different magnifications and (f) EDS chemical analysis of corrosion products.

Fig. 3 shows the potentiodynamic scanning profiles that describe the corrosion behavior in aerated solution. The polarization features were similar to the commonly reported profiles in aerated carbonate/bicarbonate corrosion studies [24,25]. Besides, electrochemical parameters of the active dissolution region, corrosion potential (E_{corr}), corrosion current density (I_{corr}), anodic Tafel slope (β_a), and cathodic Tafel slope (β_c) are reported in Table 2. These parameters were calculated by CView software and values had been confirmed by the conventional method of drawing lines along the curves of the plots. The other parameters containing passivation potential (E_{pass}), passivation current (I_{pass}), passivation potential range (ΔE_{pass}) and pitting potential (E_{pit}), which are shown in the table, had been calculated from the excel plots of the curves to obtain the exact values.

According to the test results, type A steel showed higher corrosion potentials than type B one. In contrast, the corrosion current density was less in steel A compared to steel B. The corrosion rate values for A and B steels were calculated from the corrosion current densities based on Faraday's law and they are also provided in Table 2. The estimation of the corrosion rates by means of the Tafel extrapolation technique, within the active dissolution region, showed that steel A had better corrosion resistance, by almost one third, than steel B. Both steel types had identical passive current density but pitting potential was less in steel A compared to steel B.

Figs. 4(a, b) and 5(a, b) illustrate the stereo micrographs of type A and type B API X70 steels, respectively, after potentiodynamic scanning before and after removal of corrosion products. The shape, size and density of the

Table 3
Input and output parameters along with their statistic characteristics used in the ANN-based modelings.

Parameter	Unit	Minimum	Maximum	Average	Standard deviation	Median	Variance
Input							
C	wt%	0.060	0.100	0.09021	0.01508	0.1	0.000227
Mn	wt%	1.533	2.190	1.68600	0.154739	1.66	0.023944
Nb	wt%	0	0.043	0.03483	0.015609	0.043	0.000244
Ti	wt%	0.010	0.046	0.02001	0.008608	0.02	7.41E−05
N	wt%	0	0.005	0.00089	0.001828	0	3.34E−06
Mo	wt%	0.002	0.240	0.16807	0.067815	0.19	0.004599
Ni	wt%	0	0.150	0.10065	0.052025	0.13	0.002707
Al	wt%	0	0.036	0.02076	0.008856	0.02	7.84E−05
Cu	wt%	0	0.300	0.19240	0.105265	0.25	0.011081
Cr	wt%	0	0.043	0.01703	0.008542	0.016	7.3E−05
V	wt%	0	0.050	0.00593	0.01019	0.003	0.000104
Carbon equivalent (CE_{IIW})	wt%	0.356	0.507	0.44515	0.048626	0.47	0.002365
Ferrite/pearlite	%	5	99	48.80460	20.6972	50	428.3742
Bainite/martensite	%	1	95	51.19540	20.6972	50	428.3742
Reference electrode	V_{SHE}	0.197	0.242	0.23412	0.016353	0.241	0.000267
Scan rate	mV s^{-1}	0.167	1	0.59199	0.258839	0.5	0.066998
NaCl	wt%	0	80	9.50744	20.93052	0.01	438.0868
P_{O2}	atm	0	0.200	0.05977	0.092082	0	0.008479
P_{CO2}	bar	0	1	0.43678	0.498863	0	0.248864
Temperature	°C	20	90	34.97701	21.4221	25	458.9064
Bicarbonate concentration	mol	0	1	0.24046	0.285498	0.1	0.081509
Output							
E_{corr}	mV	−890	−299	−749.332	84.55149	−751	7148.954
I_{corr}	μA cm^{-2}	0.77	280.300	55.59529	61.04731	40	3726.774

corrosion pits on the surface of steel electrodes increased from steel A to steel B. Steel A, showed a less pitting density with uniform shape and smaller size whereas the pitting density formed on the surface of steel B electrode was high and had larger size and also were inhomogeneous. Figs. 4(c–e) and 5(c–e) show the scanning electron microscopy (SEM) images acquired from the surface films/products formed on the steel electrodes after potentiodynamic tests. Figs. 4(f) and 5(f) present the energy dispersive spectroscopy (EDS) chemical analysis of surface corrosion products. The results indicate that oxygen is more than 53 at% in both steels. On the other hand, carbon in steel A is less than steel B and iron content in steel A is more than B one. It can be related to the different involving mechanisms of passive film formation and breakage.

3.2. Neural network training and testing

The input variables of the ANN models consists of the weight percent of alloying elements of *"C, Mn, Nb, Ti, N, Mo, Ni, Al, Cu, Cr, V and CE_{IIW}"*, microstructure consist of *"diffusion (ferrite/pearlite) and shear (bainite/martensite) transformations"*, corrosion cell characteristics of *"reference electrode", "scan rate", "temperature", "relative pressure of oxygen", "pressure of purged CO_2", "chloride ion"* and *"bicarbonate concentration"*. *"Corrosion current density"* and *"corrosion potential"* are considered as the outputs of the ANN models in the present study. These parameters along with their variation ranges have been summarized in Table 3. It must be mentioned that *"CE_{IIW}"* is calculated according to Eq. (1) as the following [21]:

$$CE_{IIW} = C + \frac{Mn}{6} + \frac{(Cr + Mo + V)}{5} + \frac{(Ni + Cu)}{15} \quad (1)$$

Supplementary detail on the output data characteristics are presented in Fig. 6. However, standard deviation of gathered data was considered as the criterion of categorization.

Four layer feed forward neural networks with back propagation algorithms were employed to predict the corrosion current density and potential of pipeline steels. With the use of enough hidden neurons, it could be effectively approximate any continuous nonlinear function. In the proposed models, one input layer, two hidden layers with hyperbolic sigmoid activation function and one output layer with linear activation function were used. In feed forward neural networks, weights and biases are adjusted iteratively to minimize the network performance function using a training algorithm. The commonly used performance function in these neural networks is mean square error (MSE) [26]:

$$MSE(\%) = \frac{1}{n}\sum_{i=1}^{n}(t_i - o_i)^2 \times 100 \quad (2)$$

where t_i is the examined (actual) value of ith data, o_i is the predicted value for ith data as output variable, and n is the total number of variables. Here, Bayesian regularization training algorithm is used to train the networks. In this training algorithm, weights and biases are updated with Levenberg–Marquardt optimization algorithm. The network generalization could be improved by minimizing a combination of MSE and the mean square of the network weights. Also, the weights are considered as random variables with Gaussian distribution. To improve the generalization property of proposed models the early stopping technique was used and the overall data was randomly divided into three subsets of training, testing and validating. In this technique, training process should be stopped when the error for the validation set starts to increase.

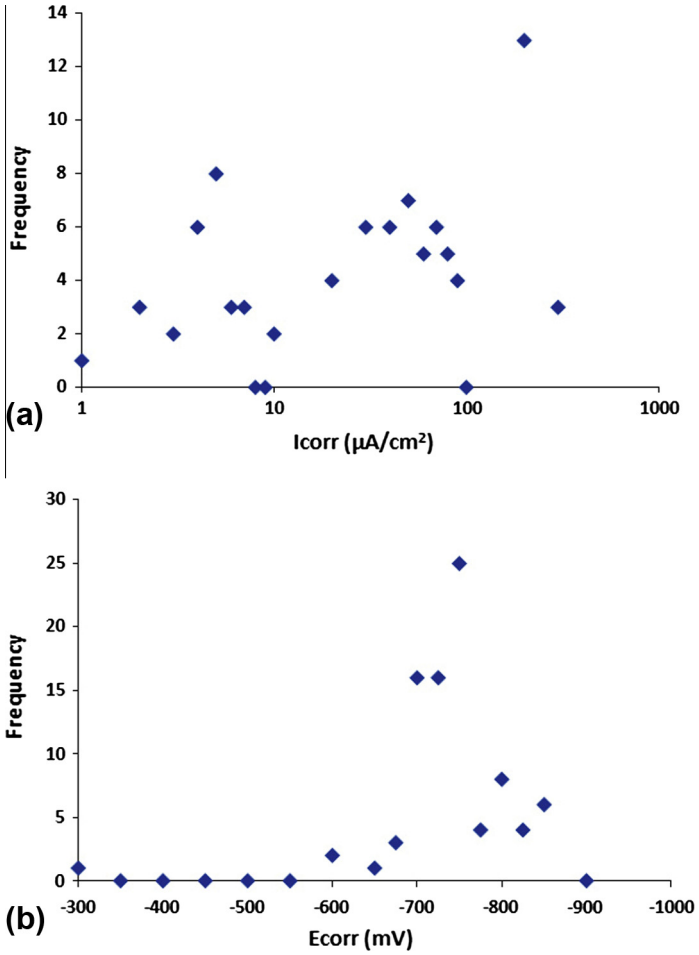

Fig. 6. Repetition frequency of (a) corrosion current density and (b) potential in 87 examined datasets.

The error value of testing shows if the over fitting has been occurred. As listed in Table 3, the collected experimental data included 87 different datasets of which 61 series (70% of total data) were used for training the network. The remained data were divided equally into two subsets containing 13 data sets (15% of total data for each) to validate and test the trained networks.

The numbers of nodes in input and output layers are equal to the number of inputs and outputs of the networks, i.e. 21 and 1 for the present work, respectively. The number of nodes in the hidden layer is obtained through trial and error during training and testing process of the networks. Usually, scatter diagrams are used to plot the predicted values of the ANNs vs. measured (experimental) ones. In this research, in addition to scatter plots, two statistical criteria (i.e. absolute fraction of variance (R^2) (according to Eq. (3) [27]) and mean relative error (MRE) (according to Eq. (4) [27]), are used to evaluate the prediction precision of the proposed models:

$$R^2 = 1 - \left(\frac{\sum_{i=1}^{n} (t_i - o_i)^2}{\sum_{i=1}^{n} (o_i)^2} \right) \tag{3}$$

$$\mathrm{MRE}(\%) = \frac{1}{n} \sum_{i=1}^{n} \left| \frac{t_i - o_i}{t_i} \right| \times 100 \tag{4}$$

where t_i, o_i and n are as defined in Eq. (2). The reliability and robustness of a neural network depend on many parameters including learning constants, activation function and random distribution of the weights in the initiation of the training process and the number of nodes in the hidden layer. The small number of nodes in the hidden layer conducts underfitting and the high number causes overfitting. Some neural networks with 12–36 nodes in their hidden layers were trained and the MRE values for training and testing datasets of these networks were calculated. It was determined that the network with 20 nodes in the first hidden layer and 12 nodes in the second hidden layer had the less MRE value for the testing data. The increase in the number of these nodes did not improve the network results for training data. So, the networks' structures in the present work are considered 21-20-12-1 representing inputs-nodes in the first hidden layer-nodes in the second hidden layer-target.

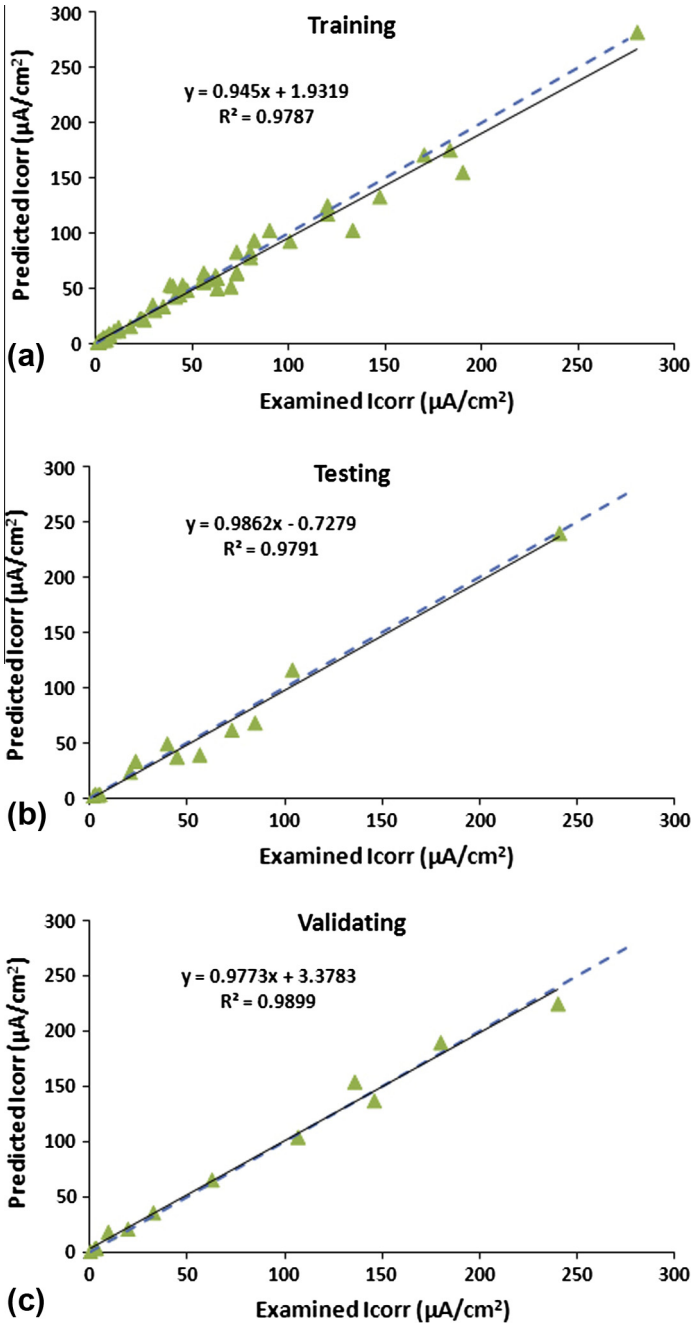

Fig. 7. The correlation of the examined and predicted corrosion current density (I_{corr}) values in (a) training, (b) testing, and (c) validating datasets using ANN-based modeling.

The traditional regression equations calculated with MINITAB® are as follows:

I_{corr} ($\mu A\ cm^{-2}$) = 1758.71 + 9751.61 C − 1017.65 Mn − 14375.4 Nb − 21929.6 Ti + 8782.86 N − 0.324396 F/P + 0.119524 NaCl − 215.172 PO_2 + 1.88959 Temperature + 108.349 Bicarbonate concentration.

E_{corr} (mV) = 3686.66 + 37054.4 C − 2861.45 Mn − 45900.2 Nb − 77753.5 Ti + 81899.1 N + 2.94359 F/P + 0.259997 NaCl + 185.097 PO_2 − 0.244578 Temperature − 88.843 Bicarbonate concentration.

The R^2 values for traditional regression analysis were 51.9% and 67.43%, respectively.

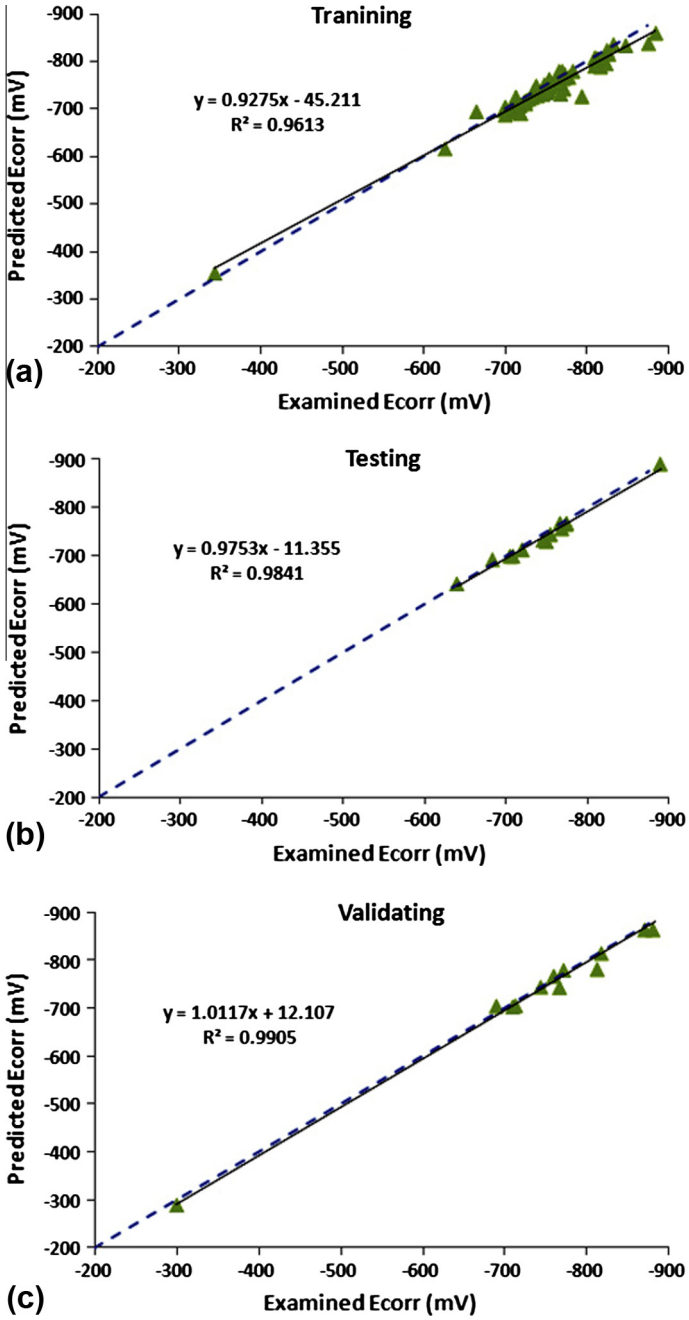

Fig. 8. The correlation of the examined and predicted corrosion potential (E_{corr}) values in (a) training, (b) testing, and (c) validating datasets using ANN-based modeling.

The results of the developed ANN-based models to predict the corrosion current density and potential of pipeline steels (in the form of scatter plots and calculated R^2 values) are shown in Figs. 7 and 8, respectively. Also, calculated MRE values for overall data and training, testing and validating subsets are presented in Table 4. As it could be seen from Figs. 7 and 8 and Table 4, the developed feed forward ANN models with R^2 upper than of 0.96 and mean relative error lower than of 20.7% for overall data could predict the corrosion current density and potential of pipeline steels with an acceptable precision. In other words, there is a good agreement between the measured (experimental)

Table 4
Calculated MRE values for training, testing and validating datasets in ANN-based modelings.

MRE	Training	Testing	Validating
E_{corr}	1.70829	1.14372	1.71622
I_{corr}	12.77667	20.72427	18.74735

corrosion current density and potential and the results of the presented models.

4. Conclusions

In this study, neural networks with feed forward topology and back propagation algorithms were used to predict the corrosion current density and potential of pipeline steels. The chemical composition and electrochemical cell parameters were considered as inputs of the networks. These were employed from a wide range database containing results of pipeline steel plates and pipes through the pilot mill and weld heat affected zone conditions. The definition of carbon equivalent (CE_{IIW}) is a novel feature of the present work that enhances the applicability of the developed ANN-based modeling. A good approximation performance with R^2 value of 0.96 and mean relative error of 20.7% for the overall data was obtained. It is concluded that there was a good agreement between the examined (experimental) and the predicted data for both corrosion current density and corrosion potential. By comparing the predicted results with the measured values, a maximum absolute relative error of 1.1% was obtained. The overall results showed that the developed models could artificially be used (as a parallel computing system) to study the effects of all input variables on the output properties.

References

[1] T. Gladman, The Physical Metallurgy of Microalloyed Steels, The Institute of Materials, London, 2002.
[2] API Specifications 5L, Specifications for Line Pipe, forty-fourth ed., American Petroleum Institute, 2007.
[3] H.F. Lopez, Effect of heat treatment on the stress corrosion resistance of a micro-alloyed pipeline steel, Corros. Sci. 41 (1999) 1037–1049.
[4] B. Lu, J. Luo, Effect of microstructure on near-neutral pH SCC resistance of pipeline steels, The Metallurgical Society of CIM, 2003.
[5] S. Koh, B. Yang, K. Kim, B. Yang, Effect of line pipe steel microstructure on susceptibility to sulfide stress cracking of line pipe steels, Corrosion (2003).
[6] R.H. Jones, R.E. Ricker, Metals Handbook, Corrosion, ninth ed., vol. 13, ASM International, 1996.
[7] R.W. Staechle, Stress corrosion cracking and hydrogen embitterment of iron base alloys, NACE-5, NACE International, Houston, 1977.
[8] F. Liu, M. Du, J. Zhang, M. Qiu, Electrochemical behavior of Q235 steel in saltwater saturated with carbon dioxide based on new imidazoline derivative inhibitor, Corros. Sci. 51 (2009) 102–109.
[9] D. Zheng, D. Che, Y. Liu, Experimental investigation on gas–liquid two phase slug flow enhanced carbon dioxide corrosion in vertical upward pipeline, Corros. Sci. 50 (2009) 3005–3020.
[10] C. Ren, D. Liu, Z. Bai, T. Li, Corrosion behavior of oil tube steel in simulant solution with hydrogen sulfide and carbon dioxide, Mater. Chem. Phys. 93 (2005) 305–309.
[11] M.E. Mohorich, J. Lamb, D. Chandra, J. Daemen, R.B. Rebak, Electrochemical studies on silicate and bicarbonate ions for corrosion inhibitors, Metall. Mater. Trans. A 41 (2010) 2563–2574.
[12] D.W. Stegmann, R.H. Hausler, C.I. Cruz, H. Sutanto, Laboratory studies on flow induced localized corrosion in CO_2/H_2S environments, Part I: Development of test methodology, in: Corrosion, Paper No. 5, NACE International, Houston, 1990.
[13] M. Ueda, H. Takabe, Effect of environmental factor and microstructure on morphology of corrosion products in CO_2 environments, in: Corrosion, Paper No. 13, NACE International, Houston, 1999.
[14] M. Kermani, A. Morshed, Carbon dioxide corrosion in oil and gas production – a compendium, Corrosion 59 (2003) 659–683.
[15] S. Wang, K. George, S. Nesic, High pressure CO_2 corrosion electrochemistry and the effect of acetic acid, in: Corrosion 2004, Paper No. 375, NACE International, Houston, 2004.
[16] G. Butler, H. Ison, Corrosion and Its Prevention in Water, Reinhold Publishing Corp., 1966.
[17] L. Xu, Z. Dong, H. Fan, Effect of CO_2, HCO^{-3} on the corrosion of carbon steel in oil and gas fields productive water, Nut. Gas Znd. 16 (1996) 57–69.
[18] X. Mao, X. Liu, R. Revie, Pitting corrosion of pipeline steel in dilute bicarbonate solution with chloride ions, Corrosion 50 (1994) 651–657.
[19] G. Khalaj, A. Nazari, H. Pouraliakbar, Prediction martensite fraction of microalloyed steel by artificial neural networks, Neural Network World 23 (2) (2013) 117–130.
[20] G. Khalaj, H. Pouraliakbar, Computer-aided modeling for predicting layer thickness of a duplex treated ceramic coating on tool steels, Ceram. Int. 40 (4) (2014) 5515–5522.
[21] M.J. Faizabadi, G. Khalaj, H. Pouraliakbar, M.R. Jandaghi, Predictions of toughness and hardness by using chemical composition and tensile properties in microalloyed line pipe steels, Neural Comput. Appl. (2014), http://dx.doi.org/10.1007/s00521-014-1687-9.
[22] G. Khalaj, A. Nazari, S.M. Mousavi Khoie, M.J. Khalaj, H. Pouraliakbar, Chromium carbonitride coating produced on DIN 1.2210 steel by thermoreactive deposition technique: Thermodynamics, kinetics and modeling, Surf. Coat. Technol. 225 (2013) 1–10.
[23] F.F. Elyian, Electrochemical evaluation of API-X100 pipeline steel in simulated carbon dioxide corrosion environments, PhD thesis, The University of British Columbia, 2011.
[24] F. Mohammadi, F.F. Eliyan, A. Alfantazi, Corrosion of simulated weld HAZ of API X-80 pipeline steel, Corros. Sci. 63 (2012) 323–333.
[25] M.S. Alwaranby, Chloride pitting corrosion of API X-80 and X-100 high strength low alloy pipeline steels in bicarbonate solutions, Master's thesis, The University of British Columbia, 2006.
[26] A. Nazari, F. Pacheco Torgal, A. Cevik, J.G. Sanjayan, Compressive strength of tungsten mine waste- and metakaolin-based geopolymers, Ceram. Int. 40 (4) (2014) 6053–6062.
[27] H. Pouraliakbar, A. Hosseini Monazzah, R. Bagheri, S.M. Seyed Reihani, G. Khalaj, A. Nazari, M.R. Jandaghi, Toughness prediction in functionally graded Al6061/SiCp composites produced by roll-bonding, Ceram. Int. 40 (2014) 8809–8825.